Verification of Concrete Spalling Simulation with Wave Propagation Theory

Sunao Tokura[1]

[1]Tokura Simulation Research Corporation (TSR)

1   Introduction

It is well known that spalling failure occurs when concrete walls are subjected to impact loading. This is explained by the fact that the compressive stress wave generated by the impact propagates from the front surface to the back surface and is reflected at the back surface as a tensile stress wave that exceeds the tensile strength of the concrete. Spalling failure is one of the most important failure modes in evaluating the response of concrete structures subjected to impact loading. Ansys LS-DYNA has several capabilities to simulate spalling failure, but whether the depth from the surface where spalling occurs is accurately simulated is an important indicator for predicting the actual response of the structure with high accuracy. Therefore, in this study, the accuracy of the simulation of spalling failure using LS-DYNA was investigated based on the wave propagation theory. As a result, it was confirmed that LS-DYNA could reproduce the behavior of spalling failure with high accuracy.

2   Wave propagation theory and failure criteria

Assuming a triangular shape impulsive compression wave is input from the end of a metal rod as shown in Fig. 1(a). The wave has a peak force of p and the duration time is t_0. The compressive wave propagates through the axial direction of the rod with the speed of sound of c. The speed of propagation of wave in 3-dimension is;

$$c = \sqrt{\frac{E(1-v)}{\rho(1+v)(1-2v)}} \tag{1}$$

where, E is Young's modulus, v is Poisson's ratio and ρ is the density of the material. Ideally, damping is not considered here. The wave length λ is given as;

$$\lambda = ct_0 \tag{2}$$

When the wave reaches the opposite free edge, the wave phase reverses and the tensile wave is reflected. And the state of superposition between incident and reflected waves is formed as shown in Fig. 1(b). The gradient of the impulsive wave can be written using the magnitude of the incident wave at the position x from the free edge σ_x^i as follows;

$$\frac{p}{\lambda} = \frac{\sigma_x^i}{\lambda - 2x}$$

and we obtain

$$\sigma_x^i = \frac{\lambda-2x}{\lambda}p \tag{3}$$

The magnitude of the superposed wave is given as the sum of the magnitude of the incident and the reflected waves as follows;

$$\sigma_x = -p + \sigma_x^i = -p + \frac{\lambda-2x}{\lambda}p = -\frac{2x}{\lambda}p \quad \left(x < \frac{\lambda}{2}\right) \tag{4}$$

where, the sign of compressive stress is positive and tensile stress is negative. In concrete materials, as is well known, the tensile strength is very low compared to the compressive strength. Therefore,

(a) Input and propagation of triangular impulsive wave

(b) Superposition of insident and reflected waves
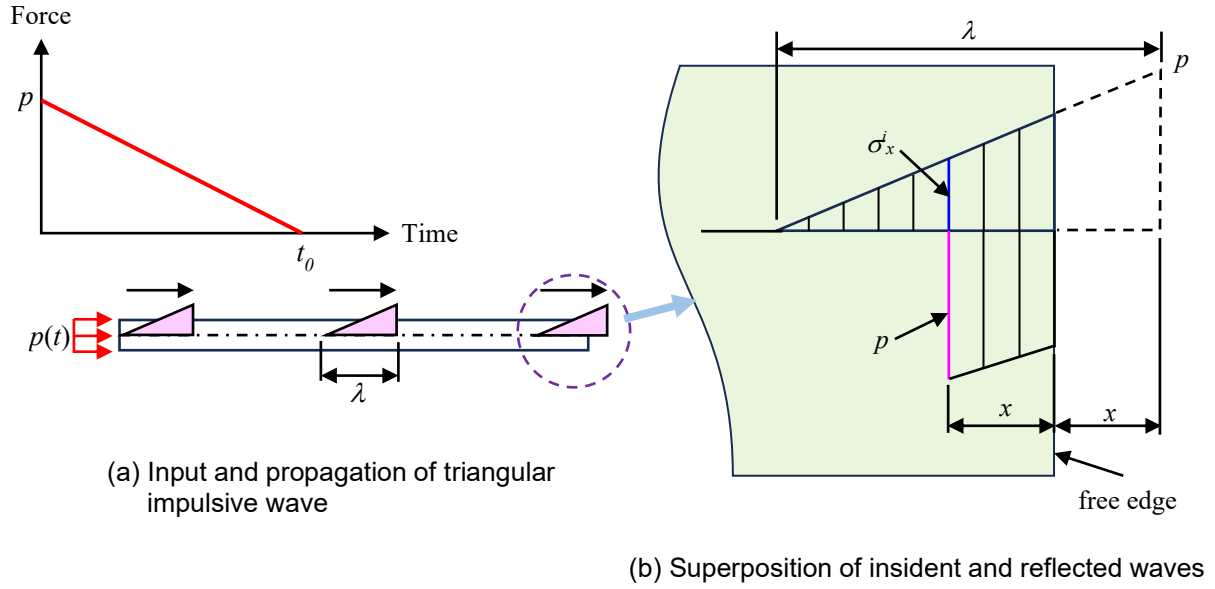
Fig.1:   Propagation of triangular impulsive compressive wave and state of reflection at free edge
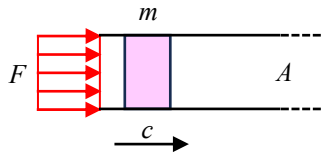
Fig.2:   Compression of small region by impact force

It is considered that spalling failure occurs when the tensile stress reaches the tensile strength f_t of the material. So, the failure criterion is given as follows;

$$\sigma_x = \frac{2x}{\lambda} p = f_t$$

From the above equation, the location of the failure x is estimated as Eq.5;

$$x = \frac{\lambda f_t}{2p} \tag{5}$$

On the other hand, the equation of motion for a small region compressed by an impact force F can be written as (see Fig. 2),

$$F = \frac{d(mv)}{dt} \tag{6}$$

where, m and v are the mass and the velocity of the small region respectively, and m is written using ρ, c, and cross section area A as follows;

$$m = \rho A c t \tag{7}$$

From Eq.6 and 7,

$$F = \frac{d}{dt}(\rho A c t v) = \rho A c v = \sigma A$$
$$\sigma = \rho c v \tag{8}$$

Once failure occurs, the debris generated is considered to scatter at a velocity v in Eq.8, so put $\sigma = p$,

$$v = \frac{p}{\rho c} \tag{9}$$

3   Analysis model

A simple concrete beam model was generated as shown in Fig. 3. The model consists of one mm cubic hexahedral elements. The element formulation is one-pint integration solid (elform=1). The number of nodes and elements are 88641 and 80000 respectively.
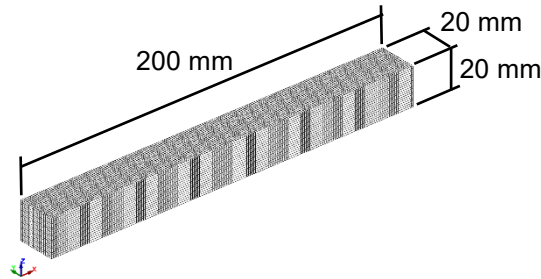
Fig.3:   Geometry and dimensions of concrete beam model

4   Analysis conditions

Figure 4 shows the analysis conditions applied to the concrete beam model. A triangular impulsive load was applied at one edge of the model. The constraint for the y-direction is defined on the nodes in the zx surface of the model and the constraint for the z-direction is defined on the nodes in the xy surface to make pseudo-one-dimensional stress wave propagation.
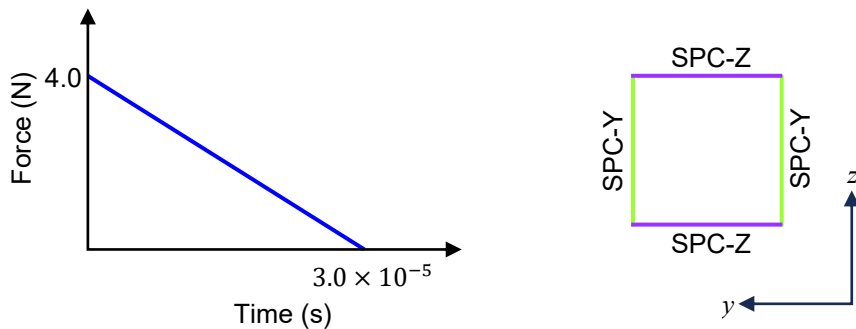
(a) Triangular impulsive force -time relation   (b) Constraint boundary condition

Fig.4:   Analysis conditions

5   Material properties and failure criteria

Two cases were investigated. In Case 1, ***MAT_WINFRITH_CONCRETE (*MAT_084)** was applied. In this case, the failure criterion is tensile strength. When induced tensile stress reaches the tensile strength, we can detect the failure location by cracks drawn on the elements. In Case 2, ***MAT_ADD_EROSION** was defined in addition to ***MAT_WINFRITH_CONCRETE** so as to generate completely separated debris. In this case, maximum principal stress was defined on ***MAT_ADD_EROSION** as the failure criterion. And a larger value was given to the tensile strength in ***MAT_WINFRITH_CONCRETE** to suppress the failure detection of this material model. The material properties and parameters are shown in Table 1.

Table 1: Material properties and numerical parameters

Material model	Case 1	Case 2	Unit
*MAT_WINFRITH_CONCRETE			
Mass density (RO)	2.3 X 10⁻⁹		ton/mm³
Initial tangent modulus of concrete (TM)	24000		MPa
Poisson's ratio (PR)	0.2		
Uniaxial compressive strength (UCS)	30.0		MPa
Uniaxial tensile strength (UTS)	3.0	5.0	MPa
Rate effect (RATE)	2.0		
Units conversion flag (CONM)	-4		
*MAT_ADD_EROSION			
Maximum principal stress at failure (SIGP1)	not used	3.0	MPa

6 Results and discussion

The scale factor for computed time step TSSFAC of 0.3 on *CONTROL_TIMESTEP was used in the simulation. As a result, the time step size yielded 8.30×10^{-8} seconds and every step was output. Figure 5 shows the shape of the stress wave obtained by the simulation when the stress wave theoretically reaches the location of 150 mm from the input edge. Using Eq. 1, the velocity of the stress wave (speed of sound) is given as 3.405×10^6 mm/s. In theory, the stress wave reaches the location of 150 mm at 4.405×10^{-5} seconds. Figure 5 shows typical stress waveforms obtained by simulation. That is, the slope of the wavefront is slightly smoother. This is thought to be due to the effect of artificial viscosity for treating discontinuous wavefront with a finite number of elements. For this reason, the wave peak position is delayed by about 5 mm compared to the theory. In terms of time, the delay is about 1.468×10^{-6} seconds. There is also a superposition of higher-order oscillations caused by local modes of vibration. The stress wave propagation and failure obtained from the simulation is shown in Fig. 6. The location of the failure can be predicted by Eq. 2 and 5;

$$x = \frac{\lambda f_t}{2p} = \frac{(ct_0)f_t}{2p} = \frac{(3.405 \times 10^6 [mm/s] \times 3 \times 10^{-5} [s]) \times 3 [MPa]}{2 \times 4.0 [MPa]} = 38.3 \, [mm]$$

For the results of the simulation, the failure occurs at 36.5 mm from the right free edge in both cases 1 and 2 (see Fig. 6). Considering the fact that the theoretical and actual stress wave peaks are deviated from each other, this is thought to be in good agreement. In addition, three cracks occur in both Cases 1 and 2, but the second and third cracks from the right seem to be caused by superposition of stress waves and local vibrations. The scattering velocity of the rightmost debris is estimated using Eq. 9 very roughly.

$$v = \frac{p}{\rho c} = \frac{4.0 \times 10^6 [N/m^2]}{2.3 \times 10^3 [kg/m^3] \times 3.405 \times 10^3 [m/s]} = 0.510 [m/s] = 510 [mm/s]$$

The rigid body velocity of the debris obtained from the simulation was 591 mm/s. In order to estimate the scattering velocity more accurately, it seems necessary to estimate the crack opening energy, etc.,
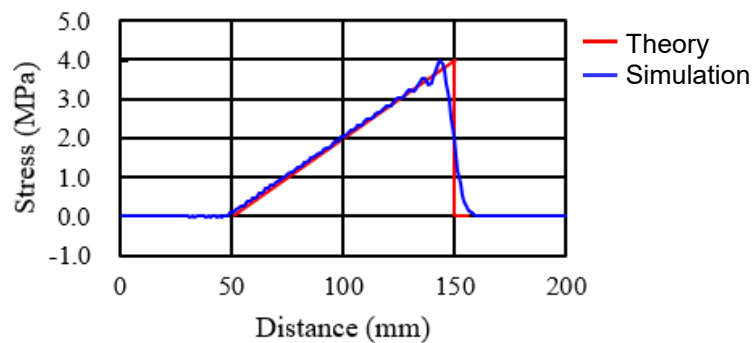
Fig.5: Stress waveform where the wavefront reaches the location of 150 mm.

Case 1: *MAT_WINFRITH_CONCRETE   Case 2: *MAT_WINFRITH_CONCRETE   x-stress
+
*MAT_ADD_EROSION
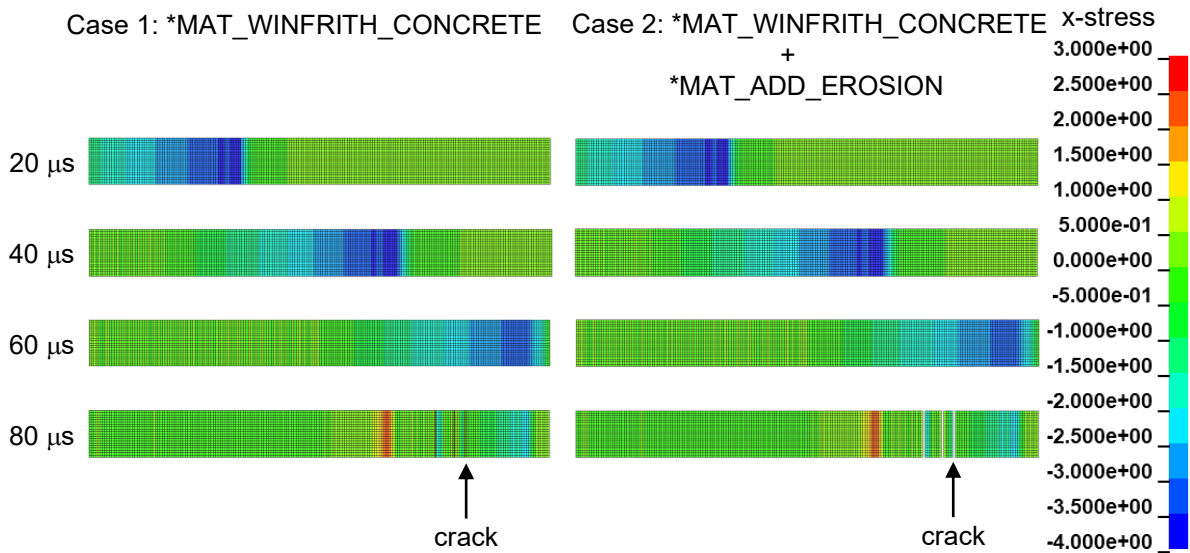
Fig.6:   Stress wave propagation and failure location

but for practical purposes, it is considered that such a rough estimation is sufficient.

7   Conclusions

In this research, the failure criteria of ***MAT_WINFRITH_CONCRETE** and ***MAT_ADD_EROSION** in LS-DYNA were compared with the classical stress wave propagation theory. As a result, the LS-DYNA simulation showed good agreement with the theory.

8   Literature

[1]   LS-DYNA® KEYWORD USER'S MANUAL VOLUME I and II, 09/24/21 (r:14186) LS-DYNA R13, LIVERMORE SOFTWARE TECHNOLOGY (LST), AN ANSYS COMPANY